Research Article | Vol. 25, No. 19 | 18 Sep 2017 | OPTICS EXPRESS 22769
Optics EXPRESS

Exploring the self-mode locking and vortex structures of nonplanar elliptical modes in selectively end-pumped Nd:YVO_4 lasers: manifestation of large fractional orbital angular momentum

J. C. TUNG,[1,2] T. OMATSU,[1,2] H. C. LIANG,[3] K. F. HUANG,[4] AND Y. F. CHEN[4,*]

[1]*Graduate School of Engineering, Chiba University, 1-33 Yayoi-cho, Inage-ku, Chiba 263-8522, Japan*
[2]*Molecular Chirality Research Center, Chiba University, 1-33, Yayoi-cho, Inage-ku, Chiba 263-8522, Japan*
[3]*Institute of Optoelectronic Science, National Taiwan Ocean University, 2 Pei-Ning Rd., Keelung 20224, Taiwan*
[4]*Department of Electrophysics, National Chiao Tung University, 1001, Ta-Hsueh Rd., Hsinchu 30010, Taiwan*
**yfchen@cc.nctu.edu.tw*

Abstract: An end-pumped Nd:YVO_4 laser under selective pumping is used to excite lasing modes with transverse patterns performed to exhibit the characteristics of multiple spots arranged on elliptical features near degenerate cavities. The spatial distribution of elliptical lasing modes is clearly revealed to be localized on the nonplanar ray orbits, so-called nonplanar elliptical modes, which possess large fractional orbital angular momentum. Moreover, temporal dynamics for the output emission of nonplanar elliptical modes are verified to obtain self-mode-locked operation. We further numerically manifest not only the influence of radial-asymmetry distributions on the vortex structures of nonplanar elliptical modes, but also the vector field of transverse lasing modes altered with twisting phase structures in the propagation direction.

OCIS codes: (140.4050) Mode-locked lasers; (050.4865) Optical vortices; (140.3480) Lasers, diode-pumped.

References and links

1. F. Krausz, T. Brabec, and C. Spielmann, "Self-starting passive mode locking," Opt. Lett. **16**(4), 235–237 (1991).
2. H. Liu, J. Nees, and G. Mourou, "Diode-pumped Kerr-lens mode-locked Yb:KY(WO_4)$_2$ laser," Opt. Lett. **26**(21), 1723–1725 (2001).
3. A. A. Lagatsky, A. R. Sarmani, C. T. A. Brown, W. Sibbett, V. E. Kisel, A. G. Selivanov, I. A. Denisov, A. E. Troshin, K. V. Yumashev, N. V. Kuleshov, V. N. Matrosov, T. A. Matrosova, and M. I. Kupchenko, "Yb^{3+}-doped YVO_4 crystal for efficient Kerr-lens mode locking in solid-state lasers," Opt. Lett. **30**(23), 3234–3236 (2005).
4. G. Q. Xie, D. Y. Tang, L. M. Zhao, L. J. Qian, and K. Ueda, "High-power self-mode-locked Yb:Y_2O_3 ceramic laser," Opt. Lett. **32**(18), 2741–2743 (2007).
5. S. Uemura and K. Torizuka, "Kerr-lens mode-locked diode-pumped Yb:YAG laser with the transverse mode passively stabilized," Appl. Phys. Express **1**(1), 012007 (2008).
6. H. C. Liang, R. C. C. Chen, Y. J. Huang, K. W. Su, and Y. F. Chen, "Compact efficient multi-GHz Kerr-lens mode-locked diode-pumped Nd:YVO_4 laser," Opt. Express **16**(25), 21149–21154 (2008).
7. Y. F. Chen, H. C. Liang, J. C. Tung, K. W. Su, Y. Y. Zhang, H. J. Zhang, H. H. Yu, and J. Y. Wang, "Spontaneous subpicosecond pulse formation with pulse repetition rate of 80 GHz in a diode-pumped Nd:$SrGdGa_3O_7$ disordered crystal laser," Opt. Lett. **37**(4), 461–463 (2012).
8. H. C. Liang, Y. J. Huang, W. C. Huang, K. W. Su, and Y. F. Chen, "High-power, diode-end-pumped, multigigahertz self-mode-locked Nd:YVO_4 laser at 1342 nm," Opt. Lett. **35**(1), 4–6 (2010).
9. Y. F. Chen, Y. C. Lee, H. C. Liang, K. Y. Lin, K. W. Su, and K. F. Huang, "Femtosecond high-power spontaneous mode-locked operation in vertical-external cavity surface-emitting laser with gigahertz oscillation," Opt. Lett. **36**(23), 4581–4583 (2011).

#304122 https://doi.org/10.1364/OE.25.022769
Journal © 2017 Received 3 Aug 2017; revised 6 Sep 2017; accepted 6 Sep 2017; published 8 Sep 2017

Optics EXPRESS

10. H. C. Liang, Y. J. Huang, Y. C. Lin, T. H. Lu, Y. F. Chen, and K. F. Huang, "Picosecond optical vortex converted from multigigahertz self-mode-locked high-order Hermite-Gaussian Nd:$GdVO_4$ lasers," Opt. Lett. **34**(24), 3842–3844 (2009).
11. H. C. Liang, T. W. Wu, J. C. Tung, C. H. Tsou, K. F. Huang, and Y. F. Chen, "Total self-mode locking of multi-pass geometric modes in diode-pumped Nd:YVO_4 lasers," Laser Phys. Lett. **10**(10), 105804 (2013).
12. J. C. Tung, H. C. Liang, P. H. Tuan, F. L. Chang, K. F. Huang, T. H. Lu, and Y. F. Chen, "Selective pumping and spatial hole burning for generation of photon wave packets with ray-wave duality in solid-state lasers," Laser Phys. Lett. **13**(2), 025001 (2016).
13. D. R. Herriott and H. J. Schulte, "Folded optical delay lines," Appl. Opt. **4**(8), 883–889 (1965).
14. A. Owyoung, C. W. Patterson, and R. S. Mcdowell, "Cw stimulated Raman gain spectroscopy of the ν1 fundamental of methane," Chem. Phys. Lett. **59**(1), 156–162 (1978).
15. J. B. McManus, P. L. Kebabian, and M. S. Zahniser, "Astigmatic mirror multipass absorption cells for long-path-length spectroscopy," Appl. Opt. **34**(18), 3336–3348 (1995).
16. K. Krzempek, M. Jahjah, R. Lewicki, P. Stefanski, S. So, D. Thomazy, and F. K. Tittel, "CW DFB RT diode laser-based sensor for trace-gas detection of ethane using a novel compact multipass gas absorption cell," Appl. Phys. B **112**(4), 461–465 (2013).
17. R. L. Byer and W. R. Trutna, "16-μm generation by CO_2-pumped rotational Raman scattering in H_2," Opt. Lett. **3**(4), 144–146 (1978).
18. P. Rabinowitz, A. Stein, R. Brickman, and A. Kaldor, "Stimulated rotational Raman scattering from para-H_2 pumped by a CO_2 TEA laser," Opt. Lett. **3**(4), 147–148 (1978).
19. K. Midorikawa, H. Tashiro, Y. Aoki, K. Nagasaka, K. Toyoda, and S. Namba, "Room-temperature operation of a para-H_2 rotational Raman laser," Appl. Phys. Lett. **47**(10), 1033–1035 (1985).
20. W. R. Trutna and R. L. Byer, "Multiple-pass Raman gain cell," Appl. Opt. **19**(2), 301–312 (1980).
21. J. G. Xin, A. Duncan, and D. R. Hall, "Analysis of hyperboloidal ray envelopes in Herriott cells and their use in laser resonators," Appl. Opt. **28**(21), 4576–4584 (1989).
22. S. H. Cho, B. E. Bouma, E. P. Ippen, and J. G. Fujimoto, "Low-repetition-rate high-peak-power Kerr-lens mode-locked $TiAl_2O_3$ laser with a multiple-pass cavity," Opt. Lett. **24**(6), 417–419 (1999).
23. A. M. Kowalevicz, Jr., A. T. Zare, F. X. Kärtner, J. G. Fujimoto, S. Dewald, U. Morgner, V. Scheuer, and G. Angelow, "Generation of 150-nJ pulses from a multiple-pass cavity Kerr-lens mode-locked Ti:Al_2O_3 oscillator," Opt. Lett. **28**(17), 1597–1599 (2003).
24. A. Sennaroglu, J. A. M. Kowalevicz, E. P. Ippen, and J. G. Fujimoto, "Compact femtosecond lasers based on novel multipass cavities," IEEE J. Quantum Electron. **40**(5), 519–528 (2004).
25. E. Abramochkin and V. Volostnikov, "Spiral-type beams," Opt. Commun. **102**(3–4), 336–350 (1993).
26. E. G. Abramochkin and V. G. Volostnikov, "Spiral light beams," Phys. Uspekhi **47**(12), 1177–1203 (2004).
27. A. Kumar, P. Vaity, and R. P. Singh, "Crafting the core asymmetry to lift the degeneracy of optical vortices," Opt. Express **19**(7), 6182–6190 (2011).
28. V. V. Kotlyar, A. A. Kovalev, and A. P. Porfirev, "Elliptic Gaussian optical vortices," Phys. Rev. A **95**(5), 053805 (2017).
29. M. A. Bandres and J. C. Gutiérrez-Vega, "Elliptical beams," Opt. Express **16**(25), 21087–21092 (2008).
30. M. A. Bandres and J. C. Gutiérrez-Vega, "Ince-Gaussian beams," Opt. Lett. **29**(2), 144–146 (2004).
31. J. B. Bentley, J. A. Davis, M. A. Bandres, and J. C. Gutiérrez-Vega, "Generation of helical Ince-Gaussian beams with a liquid-crystal display," Opt. Lett. **31**(5), 649–651 (2006).
32. S. Lopez-Aguayo and J. C. Gutiérrez-Vega, "Elliptically modulated self-trapped singular beams in nonlocal nonlinear media: Ellipticons," Opt. Express **15**(26), 18326–18338 (2007).
33. E. G. Abramochkin and V. G. Volostnikov, "Generalized Gaussian beams," J. Opt. A, Pure Appl. Opt. **6**(5), S157–S161 (2004).
34. S. Chávez-Cerda, M. J. Padgett, I. Allison, G. H. C. New, J. C. Gutiérrez-Vega, A. T. O'Neil, I. MacVicar, and J. Courtial, "Holographic generation and orbital angular momentum of highorder Mathieu beams," J. Opt. B: Quantum Opt. **4**(2), S52–S57 (2002).
35. Y. F. Chen, T. H. Lu, K. W. Su, and K. F. Huang, "Devil's staircase in three-dimensional coherent waves localized on Lissajous parametric surfaces," Phys. Rev. Lett. **96**(21), 213902 (2006).
36. Y. F. Chen, J. C. Tung, P. Y. Chiang, H. C. Liang, and K. F. Huang, "Exploring the effect of fractional degeneracy and the emergence of ray-wave duality in solid-state lasers with off-axis pumping," Phys. Rev. A **88**(1), 013827 (2013).
37. J. C. Tung, H. C. Liang, T. H. Lu, K. F. Huang, and Y. F. Chen, "Exploring vortex structures in orbital-angular-momentum beams generated from planar geometric modes with a mode converter," Opt. Express **24**(20), 22796–22805 (2016).

1. Introduction

Techniques of self-mode locking with a decrease of cavity length for developing high-repetition-rate optical pulses is an interesting phenomenon without using active elements or saturable absorbers [1]. The efficient self-mode-locked operation has recently been realized in various diode-pumped Yb-doped [2–5] and Nd-doped [6–9] crystal lasers. In particular, the

Optics EXPRESS

self-mode-locked high-order Hermite-Gaussian (HG) modes were experimentally confirmed in a selectively diode-end-pumping scheme [10]. Moreover, it has been found that when the cavity length is adjusted to be the degenerate cavities, the self-mode locking with the simultaneously longitudinal and transverse mode locking can be achieved. To fulfill the degenerate cavities, the cavity configuration requires satisfying the degenerate condition of $\Delta f_T / \Delta f_L = P/Q$, where P and Q are co-prime integers, Δf_T is the longitudinal mode spacing, and Δf_L is the transverse mode spacing. The simultaneously self-mode locking can be seen to be a time-dependent wave packet with dynamical behaviors corresponding to the planar periodic ray trajectories inside the cavity, known as planar geometric modes [11,12]. Thus far the optical configuration producing these multipass beams has been widely used in diverse experiments, such as optical delay lines [13], absorption spectroscopy [14–16], Raman conversion [17–20], high-power laser systems [21] and low repetition rate ultrafast laser cavities [22–24].

However, the generalized multipass beams in a three-dimensional (3D) laser resonator near the degenerate cavities can be localized on the nonplanar ray orbits, described as nonplanar geometric modes. The transverse pattern of nonplanar geometric modes is performed to demonstrate the property of multiple spots arranged on the topological trajectories. The topological trajectories are altered with the relative phase ϕ between the degenerate eigenmodes from the line feature at $\phi = 0$ (i.e., planar geometric modes) through the elliptical shape in the range of $0 < \phi < \pi/2$ and to the circular form at $\phi = \pi/2$. Hence, the nonplanar geometric modes can be generally represented by nonplanar elliptical modes. More interestingly, these nonplanar elliptical modes exhibit the existence of light fields with spiral characteristics during propagation. Several properties of spiral optical beams developed by Abramochkin and Volostnikov [25,26] are of practical interest for laser technologies, medicine, and microbiology. Specifically, in recent years elliptical modes with possessing fractional orbital angular momentum (OAM) and lacking for radial symmetry have been observed to be a rapidly growing interest in the field of quantum communication to achieve high security of quantum cryptography and quantum teleportation [27–34]. It is believed that the investigation of nonplanar elliptical modes with the self-mode-locked operation and the spiral features carrying huge fractional OAM is an important step in the structure light to be exploited in numerous applications.

In this work we exploit a diode-end-pumped Nd:YVO_4 laser with selective pumping to produce the nonplanar elliptical modes near the degenerate cavities. The experimental far-field patterns of nonplanar elliptical modes with the characteristics of multiple spots reveal to obtain the self-mode locking. To analyze the average OAM and the vortex structures of nonplanar elliptical modes, we theoretically perform that spatial distributions of nonplanar elliptical modes can be perfectly reconstructed with the numerical calculations. Theoretical exploration validates the influence of radial-asymmetry distributions on the vortex structures of nonplanar elliptical modes that the primary singularities can be separated by controlling the phase factor between the degenerate eigenmodes. It is further observed that the vector field of transverse lasing modes is displayed swirling features along the elliptical structure at the beam waist, and evidently altered with the twisting phase angle field in the propagation direction.

2. Experimental results for the self-mode locking of nonplanar elliptical modes

Here we demonstrate nonplanar elliptical modes generated from nearly degenerate cavities by exploiting the selective pumping in a concave-plano resonator as shown in Fig. 1. The front mirror is a 10-mm radius-of-curvature concave mirror with antireflection coating at 808 nm on the entrance face and with high-reflectance coating at 1064 nm (>99.8%) and high transmittance coating (T>95%) at 808 nm on the second surface. The gain medium is an *a*-cut 2.0-at.% Nd^{3+}:YVO_4 crystal with a length of 2 mm. One side of the gain medium is coated for

Optics EXPRESS

antireflection at 808nm and 1064 nm (reflection < 0.1%) and the other side is coated to be an output coupler with a transmission of 0.5% at 1064 nm. The pump source is an 808-nm fiber-coupled laser diode with a core diameter of 100 μm, a numerical aperture of 0.16, and a maximum output power of 3 W. A focusing lens with 25 mm focal length and 85% coupling efficiency is used to focus the pump beam into the gain medium. The pump radius is estimated to be approximately 25 μm. We use the lens to reimage the transverse patterns at the different longitudinal positions inside the cavity.

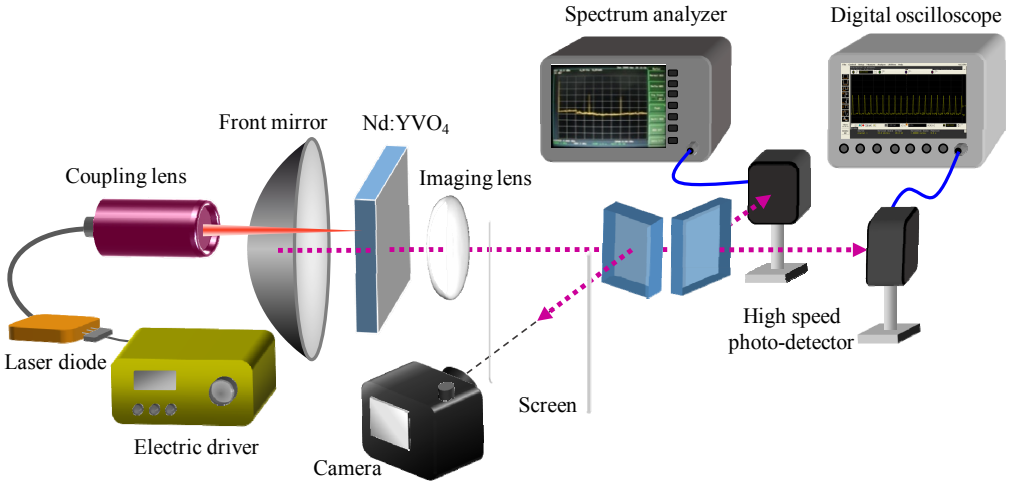

Fig. 1. Experimental setup for the self-mode-locked nonplanar elliptical modes in a concave-plano cavity with the selective pumping scheme.

When the optical cavity length L is adjusted to be approximately 11 mm and 7 mm, the measured transverse patterns at the different longitudinal positions for $(P,Q) = (1,3)$ and $(P,Q) = (1,5)$ could be obtained as shown in the upper row of Fig. 2 and Fig. 3, respectively. The z-dependent experimental patterns clearly display a characteristic of multiple spots well localized on elliptical shapes that is consistent with the periodic ray orbit depicted in the lower row of Fig. 2 and Fig. 3. Furthermore, the pump profile at the location of the crystal is a Gaussian distribution satisfying sufficient overlap with the noticeable bright spot of the lasing mode distribution shown in Fig. 2 for $z = -L/5$ and Fig. 3 for $z = -L/3$. Since the cavity mode possessing the biggest overlap with the gain region will dominate the laser emission, the nonplanar elliptical mode can be generated by precisely manipulating and persistently shifting the pump position on the gain medium. The experimental results of the nonplanar elliptical mode for $(P,Q) = (1,3)$ can be found under the off-center pumping with accurately transverse displacements of $\Delta x = 0.47$ mm and $\Delta y = 0.45$ mm along the x- and y- directions; the nonplanar elliptical mode for $(P,Q) = (1,5)$ is produced with $\Delta x = 0.43$ mm and $\Delta y = 0.80$ mm along the x- and y- directions, respectively. On the whole, nonplanar elliptical modes are usually difficult to be flexibly generated in the present approach that the strictly transverse displacements are required to balance the astigmatism induced by the birefringence of the gain medium and to achieve the isotropic effective cavity lengths in x- and y- directions.

Optics EXPRESS

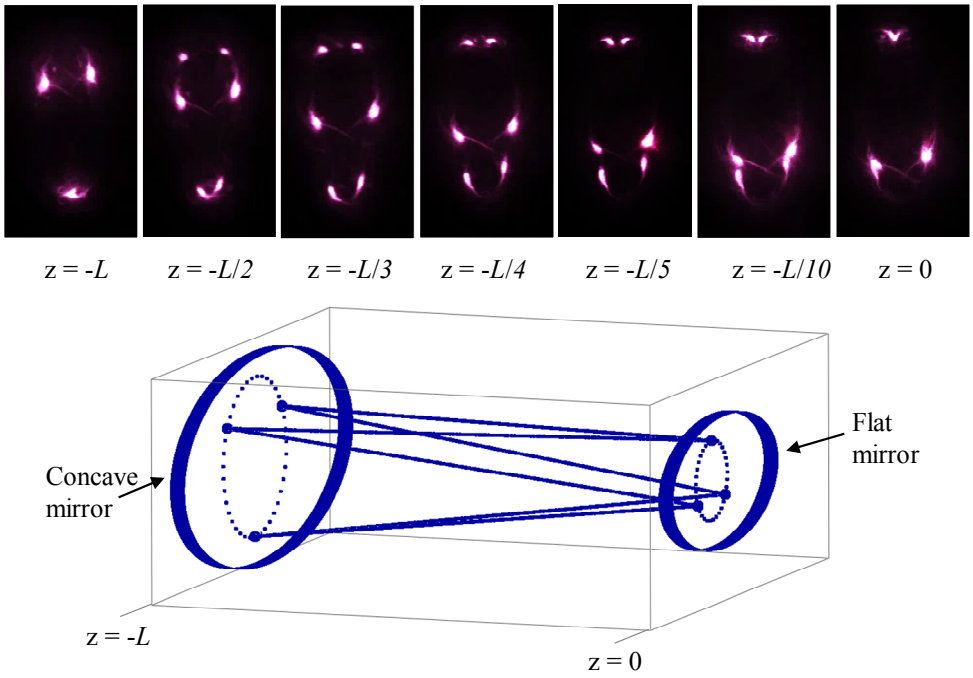

Fig. 2. Upper row: experimental transverse patterns with (P,Q) = (1,3) measured at the different longitudinal positions inside the concave-plano resonator. Lower row: periodic ray orbit in geometric optics.

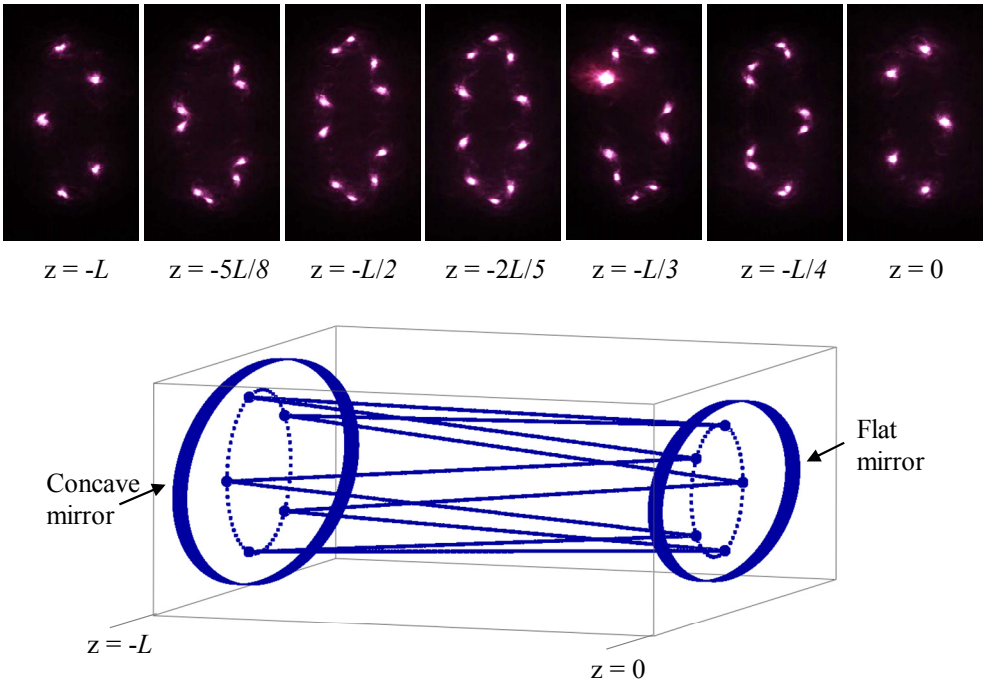

Fig. 3. Upper row: experimental transverse patterns for the case of (P,Q) = (1,5) measured at the different longitudinal positions inside the concave-plano resonator. Lower row: periodic ray orbit in geometric optics.

Optics EXPRESS

Figure 4 shows the schematic of the time-dependent photon wave packet related to the mode-locked operation with dynamical behaviors corresponding to the nonplanar elliptical modes in the laser cavity. It indicates that when the ratio $\Delta f_T / \Delta f_L$ is a simple fraction P/Q with P and Q to be co-prime integers, the wave packet inside the cavity periodically returns to its original position and direction after $(P \cdot Q)$ round trips for the round-trip time $t_r = 2L/c$. It has recently been confirmed that when the cavity length is adjusted to be the degenerate cavity, the self-mode locking can be achieved to generate a localized wave packet traveling along the planar geometric trajectories inside the cavity by identifying the relative shifts of the time sequences between different spots of the far-field pattern [11,12]. Here a similar approach is utilized to build a self-mode-locked laser in Fig. 1. The far-field patterns of nonplanar elliptical modes for $(P,Q) = (1,3)$ and $(P,Q) = (1,5)$ display a characteristic of multiple spots depicted in the insets of Figs. 5(c) and 5(d), respectively. The high-speed InGaAs photodetector (Electro-optics Technology Inc. ET-3500 with rise time 35 ps) is employed to measure the temporal behavior in different spots of the far-field pattern. The output signal of the photodetector is connected to a digital oscilloscope (Agilent DSO 80000) with 10 GHz electrical bandwidth and a sampling interval of 25 ps. The output signal of the photodetector is also analyzed by an RF spectrum analyzer (Agilent) with a bandwidth of 26.5 GHz. Figures 5(a) and 5(b) show the experimental results of the mode-locked pulse trains for one of the spots in the far-field patterns for $(P,Q) = (1,3)$ and $(P,Q) = (1,5)$ measured with a 5 GHz bandwidth real-time oscilloscope, respectively. The corresponding power spectrum is measured by an RF spectrum analyzer with a span of 26.5 GHz in Figs. 5(c) and 5(d), demonstrating the signal to noise to be greater than 35 dB. The fundamental frequency peaks can be seen to be 4.529 GHz in Fig. 5(c) and 4.289 GHz in Fig. 5(d), which correspond accurately to Δf_T shown that a wave packet returns exactly to the same position and direction after 3 and 5 round trips in the cavity, respectively. Since nonplanar elliptical modes require simultaneously longitudinal and transverse mode locking, the mode-locked condition is certainly more rigorous than fundamental modes with purely longitudinal mode locking. Even though the performance of mode locking for nonplanar elliptical modes is not perfect as the fundamental modes, it can be seen that the pulse trains display full modulation without CW background, indicating that the mode-locked operation is achieved. It is worthwhile to mention that the above results are all for the isotropic effective cavity lengths in x- and y-directions inside the laser resonator. To increase the effective path length exploited in numerous applications, the present approach can be further justified to introduce an appropriate astigmatism into the laser cavity to achieve mode-locked states corresponding to nonplanar periodic ray orbits with marvelous structures.

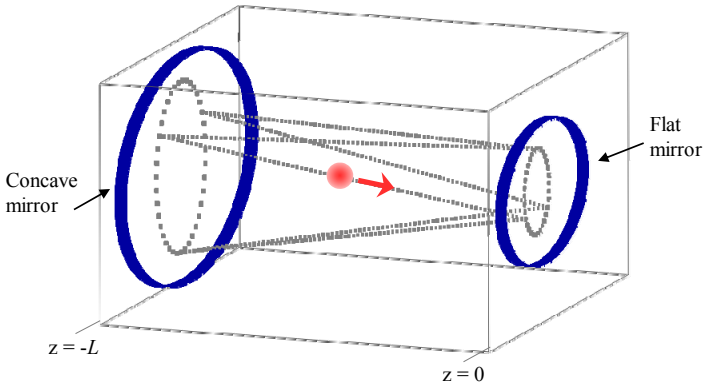

Fig. 4. Schematic of the time-dependent photon wave packet related to the mode-locked operation with dynamical behaviors corresponding to the nonplanar elliptical modes in the laser cavity.

Optics EXPRESS

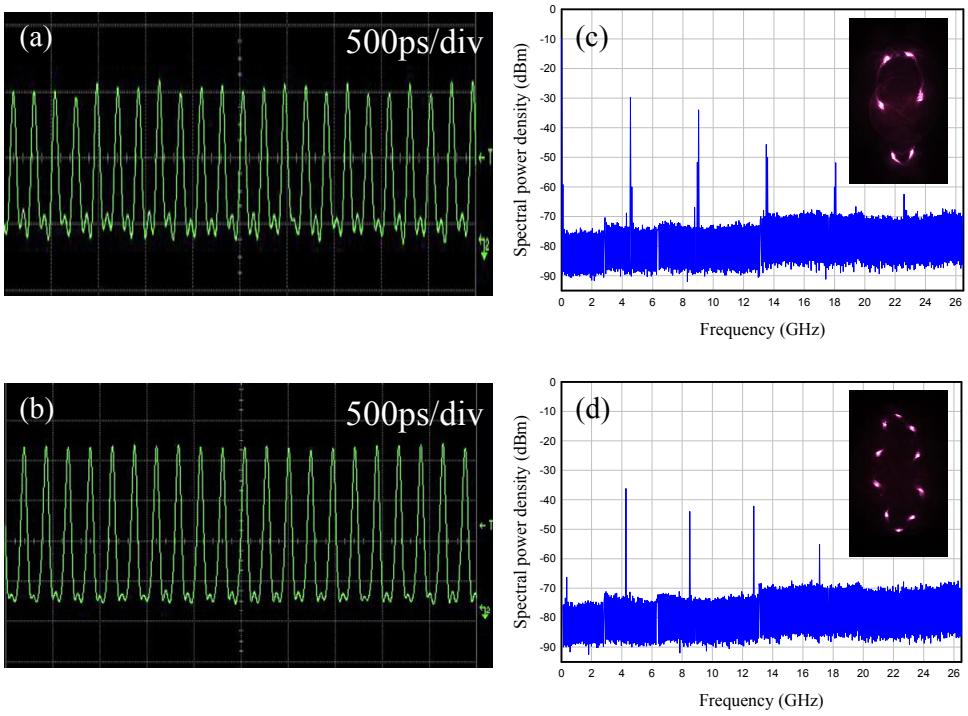

Fig. 5. Real-time trace of pulse train for the case of: (a) (*P*,*Q*) = (1,3); (b) (*P*,*Q*) = (1,5). RF power spectrum of the pulse train (the inset: transverse far-field pattern) for the case of: (c) (*P*,*Q*) = (1,3); (d) (*P*,*Q*) = (1,5).

3. Theoretical analysis of vortex structures generated from nonplanar elliptical modes

Considering the paraxial approximation, the eigenmodes for the laser cavity with a concave mirror at $z = -L$ and a plane mirror at $z = 0$ can be divided into two waves traveling in opposite directions: $\Phi_{m,n,\ell} = [\Phi^{(+)}_{m,n,\ell} + \Phi^{(-)}_{m,n,\ell}]/\sqrt{2}$, where

$$\Phi^{(\pm)}_{m,n,\ell}(x,y,z) = \psi_{m,n}(x,y,z)\, e^{-i\left[k_{m,n,\ell}\,\tilde{z} \mp (m+n+1)\theta_G(z)\right]} e^{\pm i\pi/2}, \tag{1}$$

the transverse distribution $\psi_{m,n}(x,y,z)$ is the HG mode:

$$\psi_{m,n}(x,y,z) = \frac{\sqrt{2}}{w(z)}\left(2^{m+n} m!n!\pi\right)^{-1/2} e^{-(\tilde{x}^2+\tilde{y}^2)/2} H_m(\tilde{x}) H_n(\tilde{y}), \tag{2}$$

$H_n(\cdot)$ is the Hermite polynomials, $\tilde{x} = \sqrt{2}\xi_x / w(z)$, $\tilde{y} = \sqrt{2}\xi_y / w(z)$, $\xi_x = (x+y)/\sqrt{2}$, $\xi_y = -(x-y)/\sqrt{2}$, $\tilde{z} = z\left[1 + (x^2+y^2)/2(z^2+z_R^2)\right]$, $w(z) = w_o\sqrt{1+(z/z_R)^2}$, w_o is the beam radius at the waist, $z_R = \pi w_o^2/\lambda$ is the Rayleigh range, $k_{m,n,\ell}$ is the eigenvalue of the wave number, ℓ is the longitudinal mode index, m and n are the transverse mode indices, and $\theta_G(z) = \tan^{-1}(z/z_R)$ is the Gouy phase. For the concave-plano resonator, the longitudinal and transverse mode spacings are respectively given by $\Delta fL = c/2L$ and $\Delta f_T = (\Delta f_L/\pi)\sin^{-1}\sqrt{L^*/R}$, where $L = L_c + (n_r - 1)L_g$, $L^* = L_c + [(1/n_r) - 1]L_g$, Lc is the

Optics EXPRESS

geometrical length of the cavity, *Lg* is the length of the gain material, and *nr* is the refractive index of the gain medium. In terms of ΔfL and ΔfT, the eigenvalue $k_{m,n,\ell}$ is given by $k_{m,n,\ell} = (\pi / L)\left[\ \ell + (m+n+1)(\Delta f_T / \Delta f_L)\right]$. Here the components of $\Phi^{(+)}_{m,n,\ell}$ and $\Phi^{(-)}_{m,n,\ell}$ denote the waves traveling backward and forward in the cavity, respectively. With the longitudinal and transverse mode spacings depending on the optical cavity length *L*, nonplanar elliptical modes can be constructed in degenerate cavities satisfying the condition of $\Delta fT / \Delta fL = P/Q$ by adjusting the optical cavity length *L,* where *P* and *Q* are co-prime integers. In terms of the traveling components $\Phi^{(\pm)}_{m,n,\ell}$ and the degenerate conditions of $\Delta fT / \Delta fL = P/Q$, the wave distributions of lasing modes in a standing-wave cavity can be expressed as a sum of two traveling waves [35]: $\Psi_{M,N} = [\Psi^{(+)}_{M,N} + \Psi^{(-)}_{M,N}]/\sqrt{2}$, where

$$\Psi^{(\pm)}_{M,N}(x,y,z;\phi) = \sum_{s=0}^{M} a_{M,s} \sum_{K=0}^{N+sQ} b_{N,s,K} e^{iK\phi} \Phi^{(\pm)}_{K,\,N+sQ-K,\,\ell_o - sP}(x,y,z) \tag{3}$$

$$a_{M,s} = 2^{-M/2}\left[\frac{M!}{s!(M-s)!}\right]^{1/2} \tag{4}$$

and

$$b_{N,s,K} = 2^{-(N+sQ)/2}\left[\frac{(N+sQ)!}{K!(N+sQ-K)!}\right]^{1/2} \tag{5}$$

are the weighting coefficients, and the parameter ϕ is the relative phase between the degenerate traveling components. Note that the index ℓ_o indicates the maximum longitudinal order, the integer $M + 1$ represents the total number of longitudinal eigenmodes in the lasing modes, and the integer $N = m_o + n_o$ denotes the sum of the transverse orders in *x*- and *y*-directions, where $m_o = [\Delta x / w(z_c)]^2$, $n_o = [\Delta y / w(z_c)]^2$, and z_c is the location of the gain medium [36]. In other words, the values of the parameters m_o and n_o signify the magnitudes of the off-center displacements in the *x*- and *y*- directions, respectively. For the frequency peak corresponding to Δf_T in Fig. 5, it means a unidirectional wave packet traveling along the nonplanar geometric trajectories as seen in Fig. 4 that implies the traveling waves $\Psi^{(+)}_{M,N}$ and $\Psi^{(-)}_{M,N}$ with the same phase factor ϕ. Therefore, the relationship between m_o, n_o and ϕ is given by the expression for OAM: $\hbar\,(m_o + n_o)\sin\phi$. With the transverse orders m_o and n_o in *x*- and *y*- directions to be the integers closest to the values of $[\Delta x / w(z_c)]^2$ and $[\Delta y / w(z_c)]^2$, the parameters m_o and n_o can be shown as 124 and 113 for (*P*,*Q*) = (1,3) in Fig. 2 with Δx = 0.47 *mm*, Δy = 0.45 *mm* and z_c = –2 *mm*. With the same parameter z_c, the transverse orders can be verified to be m_o = 103 and n_o = 359 for (*P*,*Q*) = (1,5) in Fig. 3 with Δx = 0.43 *mm* and Δy = 0.80 *mm.* The parameter ϕ is provided with $\pi/5$ due to the ellipticity of the lasing modes in Fig. 2 and Fig. 3. Therefore, the average OAM can be calculated as $139.3\,\hbar$ and $255.1\,\hbar$ for (*P*,*Q*) = (1,3) in Fig. 2 and (*P*,*Q*) = (1,5) in Fig. 3, respectively, which indicate the large fractional OAM in such beams. However, the integer *N* related to the experimental observations to be 237 for (*P*,*Q*) = (1,3) and 462 for (*P*,*Q*) = (1,5) is so high that it is difficult to be analyzed by numerical calculations. Figure 6 just reveals the numerical transverse patterns to illustrate the contours of the experimental patterns. The upper row in Fig. 6 shows the numerical results for the spatial distribution $\left|\Psi_{M,N}(x,y,z;\phi)\right|^2$ at different seven longitudinal positions inside the concave-flat resonator for the case of (*P*,*Q*) = (1,3) with *N* =

Optics EXPRESS

30, M = 20 and $\phi = \pi/5$. It can be seen that the variation of the transverse patterns on the longitudinal positions agrees very well with the experimental results shown in Fig. 2. The lower row in Fig. 6 depicts numerical transverse patterns for (P,Q) = (1,5) with the same parameters used in the first row of Fig. 6. It can be found that the numerical calculation is also in good agreement with the experimental data in Fig. 3.

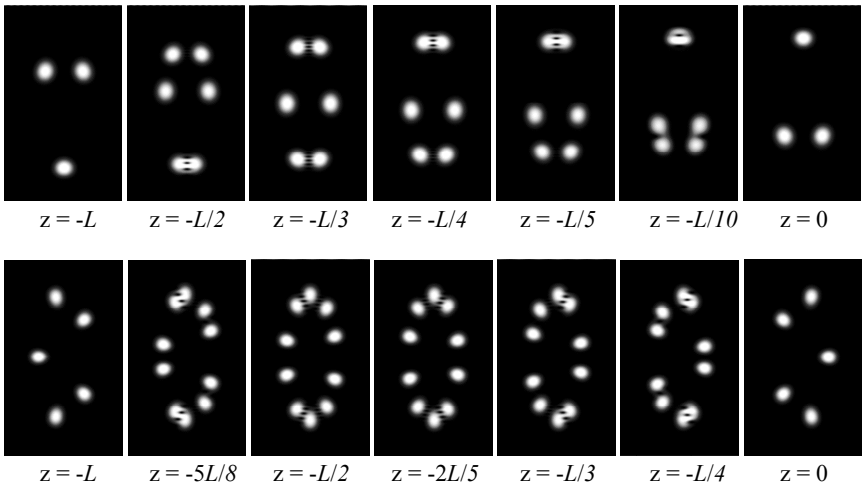

Fig. 6. Numerical transverse patterns of the spatial distribution $\left|\Psi_{M,N}(x,y,z;\phi)\right|^2$ for the cases of (P,Q) = (1,3) (upper row) and (P,Q) = (1,5) (lower row) with N = 30, M = 20, $\phi = \pi/5$ corresponding to the experimental results in Fig. 2 and Fig. 3, respectively.

In the past, the vortex structures of low-order circular geometric modes can be manifested in both experiment and theory, and the interference patterns are completely consistent with the phase structures [37]. Based on the systematically theoretical analysis for exploring the phase field of circular geometric modes, we can further investigate the intricately optical vortex beams with radial asymmetry. To verify the vortex structures of nonplanar elliptical modes, numerical results of the phase angle field are calculated by $\Theta(x,y) = \arctan\{\mathrm{Im}[\Psi_{M,N}(x,y,z;\phi)] / \mathrm{Re}[\Psi_{M,N}(x,y,z;\phi)]\}$ depicted in Figs. 7(e)-7(h), which are corresponding to the numerical patterns for various ϕ shown in Figs. 7(a)-7(d), respectively, with the parameters of (P,Q) = (1,3), $z = L$, N = 6 and M = 4. Considering the phase angle field of circular geometric modes for the case of $N > Q$ [37] as seen in Fig. 7(e), it can be found that in addition to the central singularity at the origin with the topological charges of N, there are MQ singularities surrounding on the N groups of branches outside. Figure 7(e) depicts topological charge of 6 at the centrally primary singularity, 12 secondary singularities surrounding on the 6 groups of branches outside. Moreover, it can be observed that the central singularity in Fig. 7(e) gradually splits into N primary singularities with topological charge one represented by black dots with controlling the phase factor ϕ shown in Fig. 7(e)-7(h). Although the number of secondary singularities surrounding outside is the same as the circular geometric mode, theoretical analysis reveals the distribution of the secondary singularities is somewhat different from circular geometric modes with the varying ellipticity.

Through the analytical function of $\Psi_{M,N}(x,y,z;\phi)$, the angle pattern and the transverse momentum density at different longitudinal positions inside the cavity are illustrated in the second row and the third row of Fig. 8, respectively, corresponding to the numerical patterns

Optics EXPRESS

showed in the first row of Fig. 8 with $(P,Q) = (1,3)$, $N = 15$, $M = 9$ and $\phi = \pi/3$. It is clear that the direction of momentum density displays swirling features along an ellipse at $z = 0$, and the vector field is obviously varied with the twisting phase angle field in the propagation direction. The nonplanar elliptical modes in the present method are hard to be adjusted that give rise to the inevitably high-order modes with the complex phase structures and the large angle of beam divergence shown in the first row of Fig. 2 and Fig. 3. Even though the interference pattern of nonplanar elliptical modes is difficult to be validated in the experiment, the excellent agreement of circular geometric modes between the results in Ref [37]. and Fig. 7(e) confirms the above analysis in vortex structures of nonplanar elliptical modes is reliable.

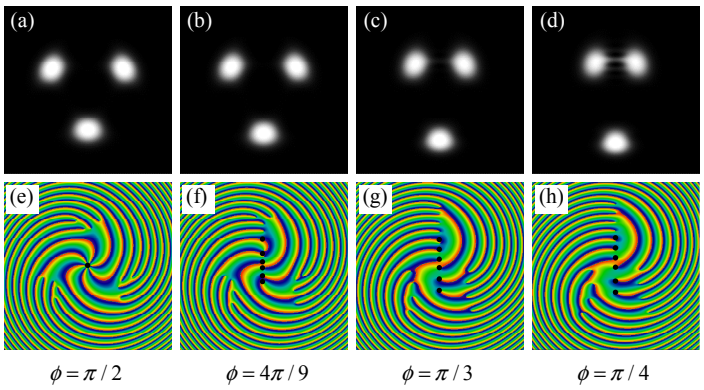

Fig. 7. Numerical calculation of the transverse pattern (upper row) and the phase angle field (lower row) for various ϕ with the parameters of $(P,Q) = (1,3)$, $z = L$, $N = 6$ and $M = 4$.

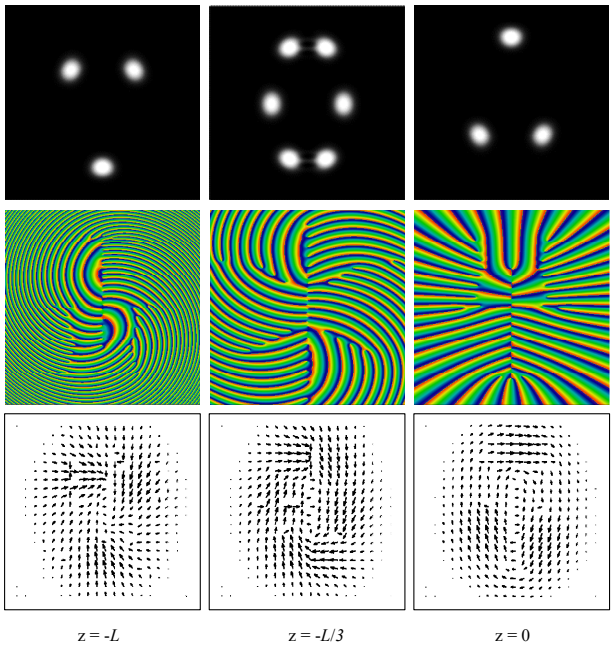

Fig. 8. Numerical calculation of the transverse pattern (first row), the phase angle field (second row) and the transverse momentum density (third row) at different longitudinal positions inside the cavity for the case of $(P,Q) = (1,3)$ with $N = 15$, $M = 9$ and $\phi = \pi/3$.

Optics EXPRESS

4. Conclusions

In summary, the diode-pumped solid-state laser under the selective pumping has been employed to excite nonplanar elliptical modes with huge fractional OAM near the degenerate cavities. The temporal dynamics for the output emission of nonplanar elliptical modes reveals to obtain the self-mode-locked states traveling along the nonplanar ray orbits inside the cavity. It has been theoretically indicated for manifesting the influence of the radial asymmetry on the vortex structures of nonplanar elliptical modes that the primary singularities can be separated by controlling the relative phase between the degenerate eigenmodes. We also numerically perform that the vector field of transverse lasing modes is displayed swirling features along an ellipse at the beam waist, and remarkably altered with the twisting phase angle field in the propagation direction.

Funding

Ministry of Science and Technology of Taiwan (Contract No. MOST 106-2628-M-009-001); Japan Society for the Promotion of Science (JSPS) Grants-in-Aid for Scientific Research (Nos. JP 15H03571 and 15K13373); Kakenhi Grant-in-Aid (No. JP 16H06507) for Scientific Research on Innovative Areas “Nano-Material Optical-Manipulation”.